First-principles study on structures and energetics of intrinsic vacancies in $SrTiO_3$

Tomohito Tanaka,[1] Katsuyuki Matsunaga,[2] Yuichi Ikuhara,[2] and Takahisa Yamamoto[1]
[1]*Department of Advanced Materials Science, Graduate School of Frontier Sciences, The University of Tokyo, 2-11-16, Yayoi, Bunkyo-ku, Tokyo 113-8656, Japan*
[2]*Institute of Engineering Innovation, The University of Tokyo, 2-11-16, Yayoi, Bunkyo-ku, Tokyo 113-8656, Japan*
(Received 17 July 2003; published 24 November 2003)

We have performed first-principles plane-wave pseudopotential calculations to study the electronic structures, structural optimization, and formation energies of intrinsic vacancies in bulk $SrTiO_3$. The anion and cation vacancy-induced levels appeared near the valence- and conduction-band edges in the band gap. The formation energies of isolated vacancies with different charge states were obtained, and the defect reaction energies, such as Sr partial Schottky ($V_{Sr}^{2-}+V_O^{2+}$), Ti partial Schottky ($V_{Ti}^{4-}+2V_O^{2+}$), and full Schottky ($V_{Sr}^{2-}+V_{Ti}^{4-}+3V_O^{2+}$) were also evaluated. It was found that depending on the atomic chemical potentials, the relative stability of the defect species or reactions is different. The overall trend of the stable defect structures can explain the electrical conductivity of $SrTiO_3$ for different chemical environments experimentally observed.

DOI: 10.1103/PhysRevB.68.205213 PACS number(s): 61.72.Ji, 61.72.Bb, 71.15.Dx

I. INTRODUCTION

Strontium titanate ($SrTiO_3$) is often used for functional electroceramic devices with a wide range of technological applications.[1–3] Pure $SrTiO_3$ is an electrical insulator with a wide band gap [3.3 eV (Ref. 4)] at room temperature. However, it is known that the electrical conductivity of $SrTiO_3$ ceramics varies with the dopant type,[5,6] Sr/Ti atomic ratio,[7] and thermal treatment conditions.[6–13] For example, the electrical conductivity of donor-doped $SrTiO_3$ experimentally measured can be divided into three regions, depending on the oxygen partial pressure (P_{O_2}).[10] At the low-P_{O_2} region, the conductivity is mostly controlled by the concentration of oxygen vacancies, while by the donor concentration at the intermediate P_{O_2} region. At the higher-P_{O_2} region, donors can be compensated by cation vacancies to decrease its conductivity. This indicates that the electrical properties of $SrTiO_3$ due to intrinsic vacancies are very sensitive to the electronic and chemical environments of the whole system. Therefore, it is necessary to understand the energetically favorable defect species and reactions in $SrTiO_3$ in detail to control and analyze the electrical properties of $SrTiO_3$.

So far, several researchers have studied to evaluate the formation energies of intrinsic point defects in undoped $SrTiO_3$,[14,15] mainly using static lattice calculations with empirical or semiempirical interatomic potentials. These studies showed that the Schottky-type defect reaction ($V_{Sr}^{2-}+V_{Ti}^{4-}+3V_O^{2+}$) has much smaller formation energy than the Frenkel-type defects such as $Sr_i^{2+}+V_{Sr}^{2-}$, $Ti_i^{4+}+V_{Ti}^{4-}$, and $O_i^{2-}+V_O^{2+}$. Moreover, Akhtar *et al.*[14] found that the formation energy of a Sr partial Schottky ($V_{Sr}^{2-}+V_O^{2+}$) is slightly smaller than that of the Schottky ($V_{Sr}^{2-}+V_{Ti}^{4-}+3V_O^{2+}$), suggesting the experimental tendency of Sr deficiency in $SrTiO_3$ at a high temperature. Thus the vacancies play an important role for the electrical properties of $SrTiO_3$.

In contrast, first-principles calculations, which are a more accurate computational technique, have been also performed for $SrTiO_3$.[16–20] Concerning the energetics of point defects in $SrTiO_3$, Astala *et al.* employed the plane-wave-based pseudopotential method to study the oxygen vacancy.[20] They took account of various charge states of V_O and found that the fully ionized state as V_O^{2+} has the smallest formation energy among them. However, they did not consider cation vacancies of V_{Sr} and V_{Ti}. Thus it cannot be concluded which type of defect species or reactions is energetically favorable in $SrTiO_3$. In addition, as stated before, it is thought that stable defect species or reactions in $SrTiO_3$ depend on the experimental environment (oxidizing or reducing atmosphere). Therefore, in order to understand the relationship between defect structures and electrical properties in $SrTiO_3$, it is important to theoretically reveal the energetics of point defects in various chemical environments.

In this study, the first-principles calculations were carried out to reveal the electronic and atomic structures of cation and anion vacancies in $SrTiO_3$. By using a rather large supercell, characteristic electronic states and formation energies of intrinsic vacancies were investigated in a first-principles manner. Considering possible defect reactions due to vacancies, the theoretically calculated reaction energies were compared with available experimental and computational results reported previously.

II. METHODOLOGY

A. Pseudopotentials and supercells

In this study, first-principles plane-wave-based calculations within the local density approximation (LDA) were performed using the VASP code.[21,22] Kohn-Sham equations were solved self-consistently using an iterative matrix diagonalization method based on a conjugate gradient technique.[23,24] For the exchange-correlation potential, the function of Ceperley and Alder as parametrized by Perdew and Zunger was used.[25,26]

Vanderbilt ultrasoft pseudopotentials were used to reduce the number of plane waves necessary to describe properties

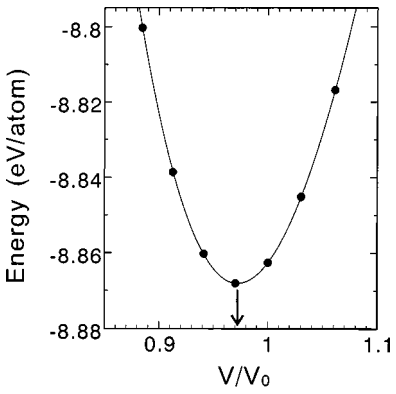

FIG. 1. Calculated total energies of perfect $SrTiO_3$ per unit cell as a function of volumes, where V_0 is the experimental volume. The curved line was fitted to the Murnaghan equation of the state (Ref. 30).

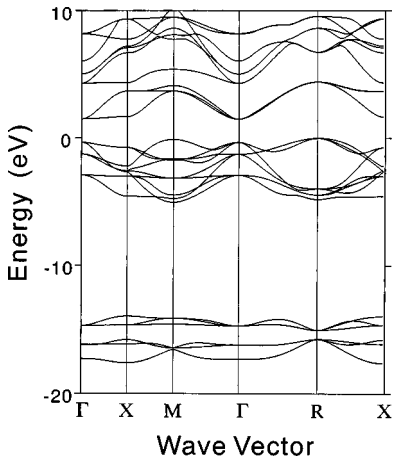

FIG. 2. Calculated energy band structure for bulk $SrTiO_3$. The VBM at R was set at 0 eV.

of material systems with a good accuracy.[27,28] For O, $2s^2$ and $2p^4$ electrons were considered as valence electrons, while $5s^2$ electrons were treated as valence electrons in the Sr pseudopotential. The ultrasoft pseudopotential of Ti was generated from the atomic configuration of $[\mathrm{Ar}]3d^3 4s^1$, where the $3p^6$ semicore electrons were explicitly considered as a part of the valence. Before going to supercell calculations for vacancies, test calculations were carried out by using the ultrasoft pseudopotentials for perfect $SrTiO_3$ (cubic, $Pm3m$). In the calculation, the $10\times10\times10$ k-point mesh generated by the Monkhorst-Pack scheme[29] (35 irreducible k points) was used for numerical integrations over the Brillouin zone.

Figure 1 shows calculated results of the total energies against unit-cell volumes for perfect $SrTiO_3$ at a plane-wave cutoff energy (E_{cut}) of 395.7 eV. The optimized lattice constant and the bulk modulus thus obtained are listed in Table I. Our LDA calculations reproduce well the experimental data[31] (0.95% for the lattice constant and 5.46% for the bulk modulus), which are also in good agreement with theoretical results[16,32] previously reported.

Figure 2 shows the calculated band structure of perfect $SrTiO_3$. The valence-band maximum (VBM) composed of O $2p$ orbitals is located at the R point, and the VB top at M is also very close to the VBM at R. On the other hand, the conduction-band minimum (CBM) composed of Ti $3d$ orbitals is at Γ point. The bottom of the CB at X is by 0.12 eV higher than the CBM at Γ. The indirect gap between R and Γ is 1.49 eV, and the direct gap at Γ is 1.82 eV. Such a feature of the band structure agrees well with the previous LDA calculations.[16–18] However, the predicted band gap is well below the experimental value of 3.3 eV. This difference in E_g could affect the formation energies of vacancies,[33] which will be discussed later.

TABLE I. Calculated lattice constant and bulk modulus of perfect $SrTiO_3$ obtained from Fig. 1.

	Lattice constant (Å)	Bulk modulus (GPa)
This work	3.87	193
Experimental	3.905[a]	183[a]
LDA	3.87,[b] 3.86[c]	194,[b] 215[c]

[a]Reference 31.
[b]Reference 16.
[c]Reference 32.

Based on the optimized structure of perfect $SrTiO_3$, the unit cell was repeated by $3\times3\times3$ in the x, y, and z directions, and a cubic supercell containing 135 atoms was used for vacancy calculations. To introduce an isolated vacancy of Sr, Ti, and O, an interior atom was removed from the supercell. In order to take account of lattice relaxation around a vacancy, atoms within third nearest-neighbor (NN) sites from a vacancy were allowed to relax. Then atomic relaxation was performed until residual forces of relaxed atoms were less than 0.1 eV/Å. In the supercell calculations, numerical integrations over the Brillouin zone were performed only at the Γ point because of the large size of supercells. The E_{cut} value of the supercell calculations was selected at 395.7 eV. In order to confirm total-energy convergence with respect to E_{cut} values, supercell calculations of vacancies were also performed at $E_{\mathrm{cut}}=600$ eV. Then the formation energies of vacancies at $E_{\mathrm{cut}}=395.7$ eV were found to converge within 0.1 eV, so that the choice of $E_{\mathrm{cut}}=395.7$ eV is sufficient to discuss relative stability of vacancies in $SrTiO_3$ in the present study.

B. Defect formation energies

The formation energies of vacancies in $SrTiO_3$ were calculated from total energies of the supercells, based on the standard formalism by Zhang and Northrup.[34] For compound systems, formation energies of vacancies depend on the atomic chemical potentials. In addition, formation energies of charged defects also vary with the electron chemical potential—i.e., a Fermi energy. For a vacancy with a charge state q, the formation energy is given by

$$E_f = E_T(\mathrm{defect}{:}q) - N_{\mathrm{Sr}}\mu_{\mathrm{Sr}} - N_{\mathrm{Ti}}\mu_{\mathrm{Ti}} - N_{\mathrm{O}}\mu_{\mathrm{O}} + q(\varepsilon_F + E_{\mathrm{VBM}}), \quad (1)$$

where $E_T(\text{defect}:q)$ is the total energy of the supercell containing a vacancy in a charge state q. Here N_{Sr}, N_{Ti}, and N_{O} are the number of Sr, Ti, and O atoms in the supercell. μ_{Sr}, μ_{Ti}, and μ_{O} are the atomic chemical potentials, and ε_F is the Fermi energy measured from the VBM. In the supercell calculation for an isolated vacancy in $SrTiO_3$, Eq. (1) can be rewritten using a total energy of the perfect $SrTiO_3$ supercell $E_T(\text{perfect})$ as follows:

$$E_f = E_T(\text{defect}:q) - \{E_T(\text{perfect}) - n_{\text{Sr}}\mu_{\text{Sr}} - n_{\text{Ti}}\mu_{\text{Ti}} - n_{\text{O}}\mu_{\text{O}}\} + q(\varepsilon_F + E_{\text{VBM}}). \quad (2)$$

Here n_{Sr}, n_{Ti}, and n_{O} are the numbers of Sr, Ti, and O atoms removed from the perfect supercell to introduce an isolated vacancy. For each vacancy species, its charge state q varying from neutral to fully ionized states was considered: from -2 to 0 for a Sr vacancy (V_{Sr}), from -4 to 0 for a Ti vacancy (V_{Ti}), and from 0 to $+2$ for an O vacancy (V_{O}).

As can be seen in Eq. (2), E_{VBM} should be determined from supercell calculations in order to obtain the formation energy of a charged vacancy. However, it is expected that the calculated E_{VBM} value of the vacancy-containing supercell differs from that of the defect-free supercell.[35–38] This is due to the fact that the vacancy causes significant distortion to the band structure around the band gap. In such a case, it is necessary to determine E_{VBM} of the defective supercell and to line up band structures of the perfect and defective supercells. For this purpose, it was assumed that the potentials in the perfect supercell are similar to those far from a defect in a defective supercell. Then the potentials at a number of atomic sites were averaged, and the difference in the averaged potentials (V_{av}) between the perfect and defective supercells was used to determine E_{VBM} of the defective supercell as follows:[37,38]

$$E_{\text{VBM}} = E_{\text{VBM}}^{\text{perfect}} + V_{\text{av}}^{\text{defect}} - V_{\text{av}}^{\text{perfect}}. \quad (3)$$

The first term on the right-hand side of Eq. (3) can be obtained by

$$E_{\text{VBM}}^{\text{perfect}} = E_T(\text{perfect}:0) - E_T(\text{perfect}:+1), \quad (4)$$

where $E_T(\text{perfect}:q)$ indicates the total energy of a perfect supercell with the charge state q.

In the supercell calculation of charged vacancies using periodic boundary conditions, Coulomb interactions between the charged vacancies in neighboring repeated cells may occur depending on the size of supercells.[39,40] This spurious interaction of charged vacancies is necessary to be corrected in evaluating their formation energies. However, Astala *et al.* showed that the spurious interaction for oxygen vacancies in $SrTiO_3$ had converged to be less than 0.065 eV, using the 40- and 135-atom supercells.[20] Since the larger 135-atom supercells were used throughout this study, it is expected that this error is very small and does not significantly affect the present results. Thus the Coulomb correction was not used in this study.

The Fermi level ε_F in Eq. (1) varies in the range of the band gap value E_g. The band gap energy was calculated from the total energies of the supercells as

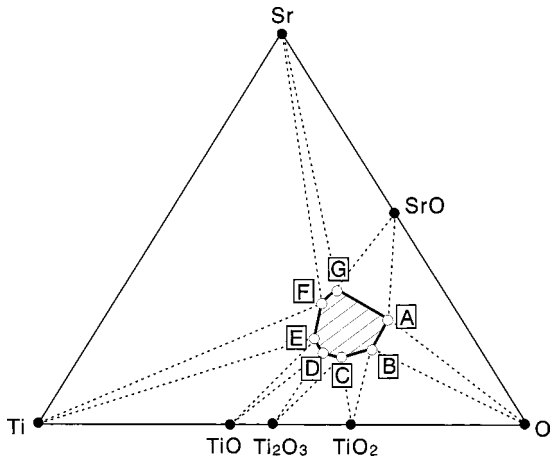

FIG. 3. Schematic phase diagram of the ternary system Sr-Ti-O.

$$E_g = E_{\text{CBM}}^{\text{perfect}} - E_{\text{VBM}}^{\text{perfect}} = \{E_T(\text{perfect}:-1) - E_T(\text{perfect}:0)\} - \{E_T(\text{perfect}:0) - E_T(\text{perfect}:+1)\}. \quad (5)$$

The calculated band gap value E_g was 1.66 eV, which is about one-half of the experimental one (3.3 eV).[4] The result that the theoretically calculated band gap is smaller than the experimental value is a commonly observed feature of the LDA, but this difference ($\Delta E_g = 1.64$ eV) is considered to affect the formation energies of vacancies in $SrTiO_3$.[33] For instance, when a vacancy has an extra level below the CBM, which is composed of cation orbitals similar to the CBM, its formation energy will be underestimated. This is because the energy position of the CBM in bulk $SrTiO_3$ is underestimated. This situation refers to the case of an oxygen vacancy in $SrTiO_3$, which will be shown later. In such a case, it could be assumed as a crude correction that the conduction band is rigidly shifted upward to match the experimental E_g. Then formation energies were corrected by adding a value of $m \times \Delta E_g$, where m is the number of electrons at vacancy-induced levels in E_g.[33] On the other hand, a formation energy of a vacancy with an acceptorlike level above the VBM was not corrected by the difference of E_g. Since such an acceptorlike level has anion-orbital character similar to the VB, the formation energy cannot be assumed to be affected by the E_g error due to the LDA.

As mentioned before, formation energies of vacancies in $SrTiO_3$ also depend on chemical potentials μ_X (X=Sr, Ti, and O). In the case of the ternary $SrTiO_3$ system, the μ_X values are determined from equilibrium conditions of various phases containing Sr, Ti, and O. Figure 3 shows the schematic phase diagram of the ternary system Sr-Ti-O. Seven points ($A-G$) indicated in the diagram correspond to the vertices of the three phase regions. It is noted that Sr-Ti binary compounds have not been so far found experimentally.[41] In the assumption that $SrTiO_3$ is always stable, the chemical potentials of the three elements can vary in the following correlation:

$$\mu_{\text{Sr}} + \mu_{\text{Ti}} + 3\mu_{\text{O}} = \mu_{\text{SrTiO}_3(\text{bulk})}, \quad (6)$$

TABLE II. Calculated and experimental enthalpies of formation for the reference materials. The values in parentheses are calculated by the spin-unpolarized method.

	Formation enthalpies (eV/atom)	
	Expt.[a]	Calc.
SrO($Fm3m$)	−3.07	−3.16 (−3.36)
TiO_2($P4_2/mmm$)	−3.24	−3.48 (−3.76)
Ti_2O_3($R\bar{3}c$)	−3.15	−3.38 (−3.63)
TiO($Fm3m$)	−2.81	−2.83 (−3.04)

[a]Reference 42.

where $\mu_{SrTiO_3(bulk)}$ is a total energy per formula unit of perfect $SrTiO_3$ crystal. At the point A in the phase diagram of Fig. 3, for example, $SrTiO_3$ is in the equilibrium with O and SrO. Thus the μ_X values are also constrained by the equations as shown below:

$$\text{point } A: \quad \mu_{Sr}+\mu_O=\mu_{SrO(bulk)}, \quad \mu_O=\mu_{O(bulk)}. \quad (7)$$

Here $\mu_{O(bulk)}$ corresponds to the chemical potential per atom of O_2 gas. From Eqs. (6) and (7), the chemical potentials of the three elements at the point A can be obtained. In a similar way, μ_{Sr}, μ_{Ti}, and μ_O at the other equilibrium points of $B-G$ can be correlated by the following equations together with Eq. (6):

$$\text{point } B: \quad \mu_O=\mu_{O(bulk)}, \quad \mu_{Ti}+2\mu_O=\mu_{TiO_2(bulk)}, \quad (8)$$

$$\text{point } C: \quad \mu_{Ti}+2\mu_O=\mu_{TiO_2(bulk)},$$

$$2\mu_{Ti}+3\mu_O=\mu_{Ti_2O_3(bulk)}, \quad (9)$$

$$\text{point } D: \quad 2\mu_{Ti}+3\mu_O=\mu_{Ti_2O_3(bulk)},$$

$$\mu_{Ti}+\mu_O=\mu_{TiO(bulk)}, \quad (10)$$

$$\text{point } E: \quad \mu_{Ti}+\mu_O=\mu_{TiO(bulk)}, \quad \mu_{Ti}=\mu_{Ti(bulk)}, \quad (11)$$

$$\text{point } F: \quad \mu_{Ti}=\mu_{Ti(bulk)}, \quad \mu_{Sr}=\mu_{Sr(bulk)}, \quad (12)$$

$$\text{point } G: \quad \mu_{Sr}=\mu_{Sr(bulk)}, \quad \mu_{Sr}+\mu_O=\mu_{SrO(bulk)}. \quad (13)$$

In order to determine the atomic chemical potentials in the above equilibrium states, total energies of the bulk systems of Sr(fcc), Ti(hcp), SrO($Fm3m$), TiO_2($P4_2/mmm$), Ti_2O_3($R\bar{3}c$), and TiO($Fm3m$) were calculated. In the case of oxygen, $\mu_{O(bulk)}$ was obtained from the total energy of the O_2 molecule using a cubic supercell $15\times15\times15$ Å^3 and only the Γ point for k-point sampling. The calculated enthalpies of formation for the reference materials together with experimental ones are shown in Table II. In this case, spin-polarized calculations were performed. As stated above, since the vacancy formation energies depend on the atomic chemical potentials, the errors in the enthalpies of formation for the reference materials due to spin-polarized and -unpolarized calculations also affect the vacancy formation energies. In order to check the errors, the spin-unpolarized calculations for the reference materials were also carried out. It can be seen in Table II that the spin-polarized calculations give more comparable enthalpies of formation with experimentally obtained values. Therefore, spin-polarized results of the reference materials were used in the present study to determine the atomic chemical potentials. In contrast, the spin polarization was not taken into account in the present vacancy-containing supercell calculations. For example, the spin-polarized calculation was also performed for the Ti vacancy of V_{Ti}^{3-}, and the difference in the formation energy from the spin-unpolarized calculation was found to be less than 1.0 meV, which is much smaller than the errors of enthalpies of formations as can be seen in Table II. In this study, therefore, the spin polarization was not included in the vacancy-containing supercell calculations.

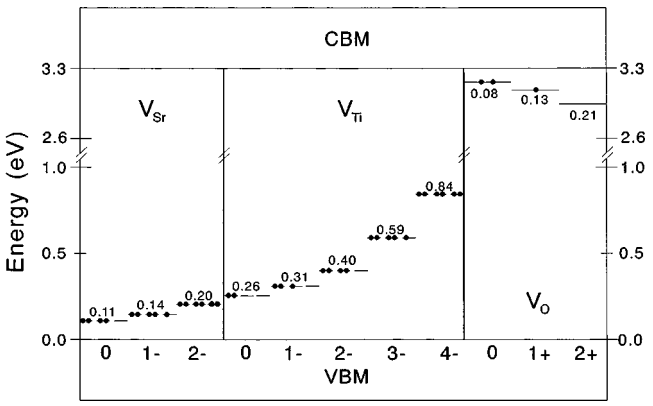

FIG. 4. One-electron energy levels for three kinds of vacancies V_{Sr}, V_{Ti}, and V_O in $SrTiO_3$ in various charge states. The positions of the one-electron energy levels are given with respect to the VBM in the cases of V_{Sr} and V_{Ti}, while those from the CBM in the case of V_O. The VBM of the perfect supercell was set at 0 eV.

III. RESULTS AND DISCUSSION

A. Atomic and electronic structures of isolated vacancies

Figure 4 shows one-electron energy levels around the band gap for vacancy-containing supercells calculated at the Γ point. The number of electrons occupying these band-gap states is also depicted. The VBM of perfect $SrTiO_3$ was set at 0 eV. The VBM positions of defective supercells were determined by the procedure described in the previous section [Eq. (3)], where the VBM energies were corrected by the average potentials. In the case of cation vacancies (V_{Sr} and V_{Ti}), the positions of the band-gap states measured from the VBM are displayed in this figure. In contrast, the energies of the band-gap states for V_O are measured from the CBM.

As can be seen in Fig. 4, each vacancy induces the extra level in the band gap. In the case of V_{Sr}, the extra levels are located near the VBM. In addition, the energetic levels become larger with increasing negative charge states. A similar feature can be also seen for V_{Ti}, although the tendency is relatively large. Figures 5(a) and 5(b) indicate contour maps of squares of wave functions for the band-gap states of V_{Sr}^0 and V_{Ti}^0 on the {100} plane, respectively. These band-gap

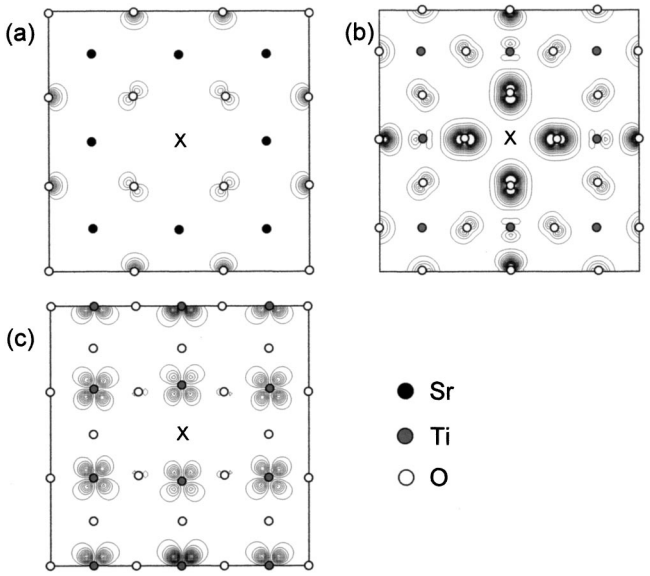

FIG. 5. Contour maps of wave functions of vacancy-induced levels of (a) $V_{Sr}{}^{0}$, (b) $V_{Ti}{}^{0}$, and (c) $V_{O}{}^{0}$ on the {100} plane of the cubic perovskite structure. The contour lines are drawn from 0.005 to 0.2 with an interval 0.01 in the unit of electrons/Å^3. The position of each vacancy is represented by "×."

states of $V_{Sr}{}^{0}$ and $V_{Ti}{}^{0}$ are mainly composed of $2p$ orbitals of O ions surrounding the vacancies, and thus these have a similar feature of the VB. It is noted that the wave function for V_{Ti} is localized more at the vacancy site than that for V_{Sr}. Due to the localized wave function of V_{Ti}, it is likely that the electrons at the level suffer from more significant electronic repulsions around the vacancy site, as compared to those at the extra level for V_{Sr}. In fact, Fig. 4 clearly shows that the energy positions for V_{Ti} with negative charges tend to become higher than those for V_{Sr}.

In contrast, the band-gap states of V_O are located close to the CBM as can be seen in Fig. 4. This level is mainly composed of Ti $3d$ orbitals as shown in Fig. 5(c). Thus this comes from the CBM as a result of V_O formation, and V_O forms a shallow donorlike state just below the CBM.

As mentioned above, the introduction of vacancies induces extra levels in the band gap. In addition, the formation of vacancies causes structural relaxations of the ions surrounding the vacancies. The distances from each vacancy to neighboring ions before and after relaxation are listed in Table III.

For all vacancy species, the first NN ions were found to exhibit outward relaxation by more than 3%, irrespective of the charge states. Such outward relaxation can be understood from the situation that the neighboring ions of a vacancy are no longer attracted by the vacancy since chemical bonds between the removed ion and surrounding ions are missing. In contrast, the second NN cations of V_{Sr} and V_{Ti} showed inward relaxation by more than 2.1%. This is due to the fact that electrostatic repulsions between second NN cations and the removed cation are reduced by the introduction of the vacancies.

As compared to the case of V_{Sr}, the relaxation of the second NN cations around V_{Ti} are more sensitive to the charge states of V_{Ti}. When the negative charge states of V_{Ti} increased, the second NN Sr ions exhibited more inward relaxations of more than 8%. This may be due to the higher-charge states of V_{Ti} (up to -4) than V_{Sr} (up to -2). Since the more charged vacancy can be considered to have electrostatic interactions with the surrounding ions at a longer distance, it is likely that the second NN Sr ions of V_{Ti} exhibited more inward relaxations toward the vacancy with increasing negative charge states of V_{Ti}.

In the case of V_O, the second NN coordination shell contains both Sr and O ions at the same distance before relaxation. After relaxation, the second NN coordination shell showed inward relaxation of about 6%. It is noted that the ions in the third NN coordination shell did not undergo significant relaxations for all vacancies, indicating that the re-

TABLE III. Distances from a vacancy to neighboring ions before and after structural relaxations of the supercells. Neighboring atomic species and their coordination numbers are also shown in brackets.

	Distance (Å) (atomic species×coordination number)		
	First NN	Second NN	Third NN
Sr (bulk $SrTiO_3$)	2.73 (O×12)	3.35 (Ti×8)	3.87 (Sr×6)
$V_{Sr}{}^{0}$	2.83	3.27	3.86
$V_{Sr}{}^{1-}$	2.83	3.28	3.86
$V_{Sr}{}^{2-}$	2.83	3.28	3.86
Ti (bulk $SrTiO_3$)	1.93 (O×6)	3.35 (Sr×8)	3.87 (Ti×6)
$V_{Ti}{}^{0}$	2.01	3.16	3.85
$V_{Ti}{}^{1-}$	2.02	3.15	3.85
$V_{Ti}{}^{2-}$	2.02	3.14	3.84
$V_{Ti}{}^{3-}$	2.02	3.11	3.84
$V_{Ti}{}^{4-}$	2.03	3.07	3.84
O (bulk $SrTiO_3$)	1.93 (Ti×2)	2.73 (Sr×4), 2.73 (O×8)	3.87 (O×6)
$V_{O}{}^{0-}$	2.06	2.86 (Sr×4), 2.56 (O×8)	3.93
$V_{O}{}^{1+}$	2.06	2.86 (Sr×4), 2.56 (O×8)	3.86
$V_{O}{}^{2+}$	2.06	2.86 (Sr×4), 2.56 (O×8)	3.86

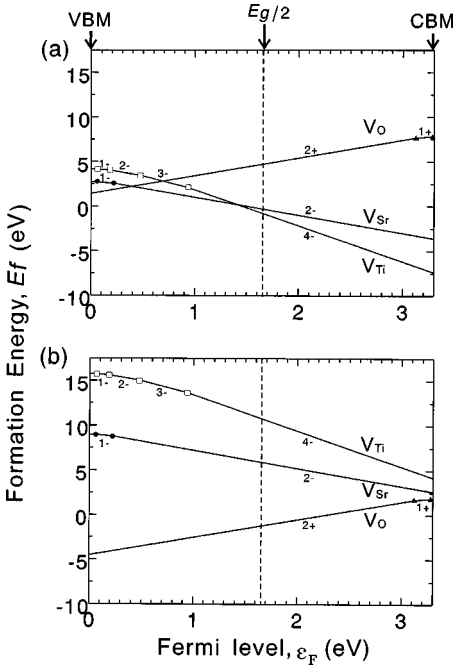

FIG. 6. Vacancy formation energies as a function of the Fermi level (a) at equilibrium point *A* and (b) *F*. For each vacancy species, only the charge state that gives the lowest formation energy with respect to the Fermi level is depicted.

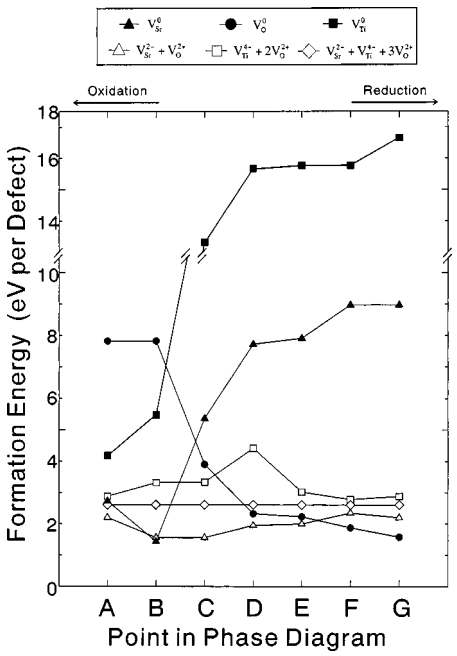

FIG. 7. Defect reaction energies and formation energies of isolated neutral vacancies in $SrTiO_3$ at each equilibrium point as indicated in Fig. 3.

laxation cutoff radius in this study is sufficient to describe the structural properties of the vacancies.

B. Formation energies

According to Eq. (2), the formation energies of isolated vacancies in $SrTiO_3$ were evaluated from the supercell calculations. As stated in the phase diagram in Fig. 3, the seven equilibrium points were considered in this study. As typical examples, the formation energies of vacancies against ε_F at points *A* and *F* are shown in Figs. 6(a) and 6(b), respectively. Since the O_2 gas phase is in equilibrium with $SrTiO_3$ and SrO at *A*, point *A* should correspond to the oxidation condition. On the other hand, $SrTiO_3$ is equilibrated with metallic Sr and Ti at point *F*, and therefore, point *F* is the reduction condition.

According to Fig. 6, the formation energies of V_{Sr}, V_{Ti}, and V_O depend on ε_F. At point *A* [Fig. 6(a)], the fully ionized charge states of ${V_{Sr}}^{2-}$, ${V_{Ti}}^{4-}$, and ${V_O}^{2+}$ are stable in a wide range of ε_F around $E_g/2$. In addition, V_{Sr} and V_{Ti} show smaller formation energies than V_O. It should be noted here that the formation energy of ${V_O}^{2+}$ becomes smaller than V_{Sr} and V_{Ti} when ε_F is located close to the VBM, which corresponds to the *p*-type environment. Since the oxygen vacancy is a shallow donor-type defect as shown in Fig. 4, that would compensate V_{Sr}, V_{Ti}, or impurities having acceptorlike levels in the band gap (see Fig. 4). This indicates the difficulty of producing *p*-type $SrTiO_3$ semiconductors, which was experimentally suggested so far.[43,44]

As for point *F* [Fig. 6(b)], the formation energies of V_{Sr} and V_{Ti} are further increased, as compared to Fig. 6(a), while that of V_O is decreased. As a result, V_O formation is easier than V_{Sr} and V_{Ti} over the entire range of ε_F. When ε_F is at $E_g/2$, which is the case of intrinsic $SrTiO_3$, the respective vacancies were found to be fully ionized. In such a case, charge neutrality of the whole system in the vacancy formation should be taken into account. As possible defect reactions due to the charged vacancies in $SrTiO_3$, the following reactions can be considered: ${V_{Sr}}^{2-}+{V_O}^{2+}$ (Sr partial Schottky reaction), ${V_{Ti}}^{4-}+2{V_O}^{2+}$ (Ti partial Schottky reaction), and ${V_{Sr}}^{2-}+{V_{Ti}}^{4-}+3{V_O}^{2+}$ (full Schottky reaction). These reaction energies can be obtained from the formation energies of the isolated vacancies, as shown in Fig. 6. It is noted here that the above Schottky-reaction energies are independent of ε_F, since the whole system of $SrTiO_3$ maintains charge neutrality even after the reactions.

Considering the phase equilibrium conditions in Fig. 3, the defect-reaction energies at each point are plotted in Fig. 7, together with the formation energies of isolated neutral vacancies. As can be seen, the reaction energies vary with the equilibrium conditions. However, the full Schottky reaction energy of ${V_{Sr}}^{2-}+{V_{Ti}}^{4-}+3{V_O}^{2+}$ was 2.61 eV, irrespective of the equilibrium conditions. This is because the whole system of $SrTiO_3$ is still stoichiometric even after the full Schottky formation. This reaction energy of 2.61 eV agrees well with the value obtained by Crawford *et al.* using static lattice calculations based on ionic pair potentials.[15] As compared to this, the Sr partial Schottky reaction of ${V_{Sr}}^{2-}+{V_O}^{2+}$ exhibited smaller energies for all equilibrium conditions, while the Ti partial Schottky reaction showed larger energies. The average value of the Sr partial Schottky reaction energy over the all equilibrium conditions (1.97 eV) is in good agreement with the experimental value 2.5 eV reported by Moos and Härdtl[10] and the theoretical one 1.53 eV obtained by Akhtar *et al.*[14]

Vacancies in the Schottky reactions have a possibility of forming a pair due to the electrostatic and elastic interactions between the vacancies. In order to estimate the effect of the defect association on the reaction energy, the supercell calculation for the Sr partial Schottky pair was performed. Assuming that V_{Sr} and V_O are located at the nearest-neighbor sites, the surrounding ions in the supercell were allowed to relax in the same manner described in the Sec. II A. It was found that the reaction energy of the associated Sr partial Schottky pair was lowered by 0.35 eV, as compared to the results in Fig. 7, which indicates the formation of the V_{Sr}-V_O pair. A similar decrease in the formation energies for the other Schottky reactions can be anticipated, so that the relative stability of the reactions is expected to be consistent with the results described above.

As can be seen from Fig. 7, neutral vacancies of V_{Sr}^0, V_{Ti}^0, and V_O^0 also vary their formation energies with the equilibrium conditions. In the case of V_{Ti}^0, its formation energy was found to be relatively high, as compared to others. Since the Ti partial reaction also has a large formation energy, it is thought that Ti vacancies are hard to be formed in $SrTiO_3$. In contrast, the formation energy of V_{Sr}^0 at point *A* was as large as that of the full Schottky reaction, and at point *B*, V_{Sr}^0 exhibited the smallest formation energy. From phase diagram of Fig. 2, points *A* and *B* correspond to the oxidation conditions ($\mu_O = \mu_{O(bulk)}$), and it can be thus said that Sr vacancies are easily formed under oxidation atmosphere. For V_O^0, its formation energy decreased in going from *A* to *G*. At points *F* and *G*, V_O^0 showed the smallest formation energy. This can be imaged from the general situation that oxygen vacancies are more easily formed under the reduction atmosphere than cation vacancies.

A number of researchers experimentally reported the behavior of the electrical conductivity of $SrTiO_3$ over a wide range of oxygen partial pressure (P_{O_2}).[6–11] At low P_{O_2}, undoped $SrTiO_3$ showed *n*-type conductivity, and the electrical conductivity decreased with increasing P_{O_2}. After passing through a minimum, the electrical conductivity of undoped $SrTiO_3$ increased again with rising P_{O_2}. From the results in Fig. 7, it was found that neutral oxygen vacancies of V_O^0 have the smallest formation energy at points *F* and *G*, so that V_O^0 defects are abundant under the small oxygen chemical potential, since the V_O^0 defect has a shallow donorlike level in the band gap (see Fig. 4) that can contribute to the *n*-type conductivity. A number of researchers also experimentally suggested the abundance of V_O under low P_{O_2},[6–11] which is consistent with our results.

In contrast, it can be seen from Fig. 7 that the Sr partial Schottky reaction is energetically favorable from points *C* to *E*, which likely correspond to intermediate P_{O_2} conditions in the experiment. As shown in Fig. 4, V_{Sr} can act as an acceptorlike defect, while V_O is a donorlike defect. As a result of the Sr partial Schottky reaction, however, the self-compensation between V_{Sr} and V_O takes place, so that the Sr partial Schottky pairs no longer contribute to increase in the electrical conductivity of $SrTiO_3$. It is considered that this situation corresponds to the experimental results where the electrical conductivity of $SrTiO_3$ undergoes a minimum value under the intermediate-P_{O_2} condition.

The increase in electrical conductivity of undoped $SrTiO_3$ under high P_{O_2}, which was experimentally observed,[10] is expected to be due to the formation of V_{Sr}^0. The present results in Fig. 7 showed that the Sr partial Schottky pairs are easily formed at the oxidation conditions of points *A* and *B*, while V_{Sr}^0 can also be present due to its relatively small formation energy. As mentioned above, the Sr partial reaction itself cannot increase the electrical conductivity because of the self-compensation, and yet neutral Sr vacancies having acceptorlike levels (see Fig. 4) can induce *p*-type conductivity. In this respect, it was suggested that Sr vacancies were predominant in $SrTiO_3$ under the oxidizing conditions in the previous experiments, where the Ruddlesden-Popper phase $SrO^*(SrTiO_3)_n$ or SrO_x enrichment acting as a source of V_{Sr} was observed.[45,46] It is noted, however, that the experimental *p*-type conductivity under high P_{O_2} was much smaller than the *n*-type conductivity under low P_{O_2},[10] corresponding to the difficulty in the *p*-type conduction of $SrTiO_3$. In order to make a quantitative comparison between theory and the observed conductivities in real $SrTiO_3$, it is necessary to estimate equilibrium concentrations of the vacancies providing charge carriers and the carrier mobility, which is, however, beyond the scope of this study.

As shown above, it was found that the present results provide a reasonable description of stable defect species and reactions in $SrTiO_3$ depending on the atomic chemical potentials, which can explain well the experimental trend in the electrical conductivity of $SrTiO_3$ over a wide range of oxygen partial pressure. It is also known that macroscopic properties of functional ceramics strongly depend on surfaces, grain boundaries, and interfaces. For example, grain boundaries can act as a sink or a source of point defects, which is explained by the space charge theory.[47–49] Due to the particular chemical environment at grain boundaries, stable defect species present at the vicinity of grain boundaries are expected to differ from those in bulk, resulting in peculiar characteristic properties of functional ceramics. In such cases, the first-principles approach using large supercells can also provide detailed information on the defect chemistry, which contributes to further understanding of various properties in ceramic materials.

IV. SUMMARY

In order to reveal the energetically favorable defect types and reactions in $SrTiO_3$, electronic structures and formation energies of intrinsic vacancies in bulk $SrTiO_3$ were investigated using first-principles pseudopotential calculations. The results obtained in this study can be summarized as follows.

(1) In the presence of vacancies (V_{Sr}, V_{Ti}, and V_O), extra levels appeared near the VBM or CBM in the band gap of $SrTiO_3$. The vacancy-induced level of V_O was found to have a shallow donor-type character, which is composed of surrounding Ti 3*d* orbitals. This indicates that the even undoped $SrTiO_3$ can become an *n*-type semiconductor by introducing V_O.

(2) Based on the formation energies of individual vacancies, the formation energies of full Schottky, Sr partial Schottky, and Ti partial Schottky reactions, which maintain charge neutrality of $SrTiO_3$, were evaluated. It was found that the calculated formation energy of Sr partial Schottky reactions was lower than that of the other defect reaction and agreed well with the previous experimental and theoretical results.

(3) The formation energies of isolated neutral vacancies and various Schottky reactions are found to vary with respect to the equilibrium condition. Concerning the calculated formation energies, the dominant defect is $V_O{}^0$ at the reduction condition, while it is the Sr partial Schottky reaction or $V_{Sr}{}^0$ at the oxidation condition. These neutral vacancies can contribute to *n*-type and *p*-type conductivities, respectively, which is in good agreement with the tendencies obtained from conductivity measurements of $SrTiO_3$ as a function of P_{O_2}.

ACKNOWLEDGMENTS

This work was supported by a Grant-in-Aid for Scientific Research from the Ministry of Education, Culture, Sports and Technology of the Japanese government.

[1] M. Fujimoto and W. D. Kingery, J. Am. Ceram. Soc. **68**, 169 (1985).
[2] M. Fujimoto, Y.-M. Chiang, A. Roshko, and W. D. Kingery, J. Am. Ceram. Soc. **68**, C300 (1985).
[3] J. Gerblinger and H. Meixner, J. Appl. Phys. **67**, 7453 (1990).
[4] T. Bieger, J. Maier, and R. Waser, Solid State Ionics **53–56**, 578 (1992).
[5] T. Yamamoto, K. Hayashi, Y. Ikuhara, and T. Sakuma, J. Am. Ceram. Soc. **83**, 1527 (2000).
[6] U. Balachandran and N. G. Eror, J. Electrochem. Soc. **129**, 1021 (1982).
[7] N-H. Chan, R. K. Sharma, and D. M. Smyth, J. Electrochem. Soc. **128**, 1762 (1981).
[8] M. B. Park and N. H. Cho, Solid State Ionics **154–155**, 175 (2002).
[9] H. Yamada and G. R. Miller, J. Solid State Chem. **6**, 169 (1973).
[10] R. Moos and K. H. Härdtl, J. Am. Ceram. Soc. **80**, 2549 (1997).
[11] R. Waser, J. Am. Ceram. Soc. **74**, 1934 (1991).
[12] T. Baiatu, R. Waser, and K. H. Härdtl, J. Am. Ceram. Soc. **73**, 1663 (1990).
[13] T. Yamamoto and Y. Ikuhara, J. Electron Microsc. **50**, 485 (2001).
[14] M. J. Akhtar, Z. Akhtar, R. A. Jackson, and C. R. A. Catlow, J. Am. Ceram. Soc. **78**, 421 (1995).
[15] J. Crawford and P. Jacobs, J. Solid State Chem. **144**, 423 (1999).
[16] S. Kimura, J. Yamauchi, M. Tsukada, and S. Watanabe, Phys. Rev. B **51**, 11 049 (1995).
[17] S-D. Mo, W. Y. Ching, M. F. Chisholm, and G. Duscher, Phys. Rev. B **60**, 2416 (1999).
[18] K. van Benthem, C. Elsässer, and R. H. French, J. Appl. Phys. **90**, 6156 (2001).
[19] N. Shanthi and D. D. Sarma, Phys. Rev. B **57**, 2153 (1998).
[20] R. Astala and P. D. Bristowe, Modell. Simul. Mater. Sci. Eng. **9**, 415 (2001).
[21] G. Kresse, Ph.D. thesis, Technische Universität, Wien, 1993.
[22] G. Kresse and J. Furthmüller, Comput. Mater. Sci. **6**, 15 (1996).
[23] I. Štich, R. Car, M. Parrinello, and S. Baroni, Phys. Rev. B **39**, 4997 (1989).
[24] M. P. Teter, M. C. Payne, and D. C. Allan, Phys. Rev. B **40**, 12 255 (1989).
[25] D. M. Ceperley and B. J. Alder, Phys. Rev. Lett. **45**, 566 (1980).
[26] J. P. Perdew and A. Zunger, Phys. Rev. B **23**, 5048 (1981).
[27] D. Vanderbilt, Phys. Rev. B **41**, 7892 (1990).
[28] G. Kresse and J. Hafner, J. Phys.: Condens. Matter **6**, 8245 (1994).
[29] H. J. Monkhorst and J. D. Pack, Phys. Rev. B **13**, 5188 (1976).
[30] F. D. Murnaghan, Proc. Natl. Acad. Sci. U.S.A. **30**, 244 (1944).
[31] *Numerical Data and Functional Relations in Science and Technology—Crystal and Solid State Physics*, edited by T. Mitsui and S. Nomura, Landolt-Börnstein, New Series, Group III, Vol. 16, Pt. a (Springer, Berlin, 1982).
[32] E. Heifets, R. I. Eglitis, E. A. Kotomin, J. Maier, and G. Borstel, Phys. Rev. B **64**, 235417 (2001).
[33] S. B. Zhang, S. H. Wei, A. Zunger, and H. Katayama-Yoshida, Phys. Rev. B **57**, 9642 (1998).
[34] S. B. Zhang and J. E. Northrup, Phys. Rev. Lett. **67**, 2339 (1991).
[35] D. B. Laks, C. G. Van de Walle, G. F. Blöchl, and S. T. Pantelides, Phys. Rev. B **45**, 10 965 (1992).
[36] A. García and J. E. Northrup, Phys. Rev. Lett. **74**, 1131 (1995).
[37] S. Pöykkö, M. J. Puska, and R. M. Nieminen, Phys. Rev. B **53**, 3813 (1996).
[38] T. Mattila and A. Zunger, Phys. Rev. B **58**, 1367 (1998).
[39] M. Leslie and M. J. Gillan, J. Phys. C **18**, 973 (1985).
[40] G. Makov and M. C. Payne, Phys. Rev. B **51**, 4014 (1995).
[41] F. N. Alidzhanov, A. V. Vakhobov, and T. D. Dushanbe, Russ. Metall. **2**, 177 (1978).
[42] *NIST Chemistry WebBook, NIST Standard Reference Database* No. 69, edited by W. G. Mallard and P. J. Linstrom (National Institute of Standards and Technology, Gaithersburg, MD, 2003).
[43] T. Higuchi, T. Tsukamoto, K. Kobayashi, S. Yamaguchi, Y. Ishikawa, N. Sata, K. Hiramoto, M. Ishigame, and S. Shin, Phys. Rev. B **65**, 033201 (2001).
[44] S. Dai, H. Lu, F. Chen, Z. Chen, Z. Y. Ren, and D. H. Ng, Appl. Phys. Lett. **80**, 3545 (2002).
[45] K. Szot and W. Speier, Phys. Rev. B **60**, 5909 (1999).
[46] K. Szot, W. Speier, U. Breuer, R. Meyer, J. Szade, and R. Waser, Surf. Sci. **460**, 112 (2000).
[47] K. L. Kliewer and J. S. Koehler, Phys. Rev. **140**, A1226 (1965).
[48] J. R. Macdonald, D. R. Franceschetti, and A. P. Lehnen, J. Chem. Phys. **73**, 5272 (1980).
[49] J. A. S. Ikeda and Y.-M. Chiang, J. Am. Ceram. Soc. **76**, 2437 (1993).